TESLA-FEL Report 2005-10

Impact of Undulator Wake-Fields and Tapering on the European X-Ray FEL Performance

Martin Dohlus, Torsten Limberg, Igor Zagorodnov

DESY, Notkestrasse 85, 22603 Hamburg, Germany

1. Introduction

The European X-ray Free-Electron Laser (XFEL) is based on self-amplified spontaneous emission (SASE) and requires an electron beam with a few kA peak current and a small-gap undulator system of up to 260 m in length [1]. The electromagnetic interaction between the high-current electron bunch and the undulator vacuum chamber affects the FEL performance.

In this paper we estimate the induced wakefields in an elliptical pipe geometry taking into account main geometrical variations of the chamber. To study the expected performance in the presence of the calculated wakefields we are doing start-to-end simulations with the codes ASTRA [2], CSRtrack [3] and Genesis [4]. In order to compensate the impact of wake fields on the FEL performance, an adiabatic change of undulator parameters is applied.

2. Start-to-Undulator Simulation

The beam dynamics in the rf photo injector and the linac has been modeled with the codes ASTRA and CSRtrack. The particles are tracked taking into account space charge effects with the code ASTRA to the 130 MeV point. For all other linac sections, transport matrices and a semi-analytic model for longitudinal space charge effects are used to propagate particle phase space. The wake field effects of the TESLA cryomodules and other elements are calculated with code ECHO [5-7] and included in the simulations. The beam dynamic in CSRtrack uses the one dimensional approach. The simulation starts with a 1nC bunch with a peak current of about 50A from the photo cathode. The bunch is compressed in two stages at 500MeV by a factor of 20 and at 2 GeV by a factor of 5. The calculated current profile and the longitudinal phase space are shown in Fig.1.

The results of this previous start-to-end simulation have been checked with a more thorough approach, where all linac sections up to 3 GeV have been calculated with ASTRA and the compressor chicanes with a 3D method in CSRtrack and the differences in the final particle distribution were not big enough to have an impact on the results of this paper.

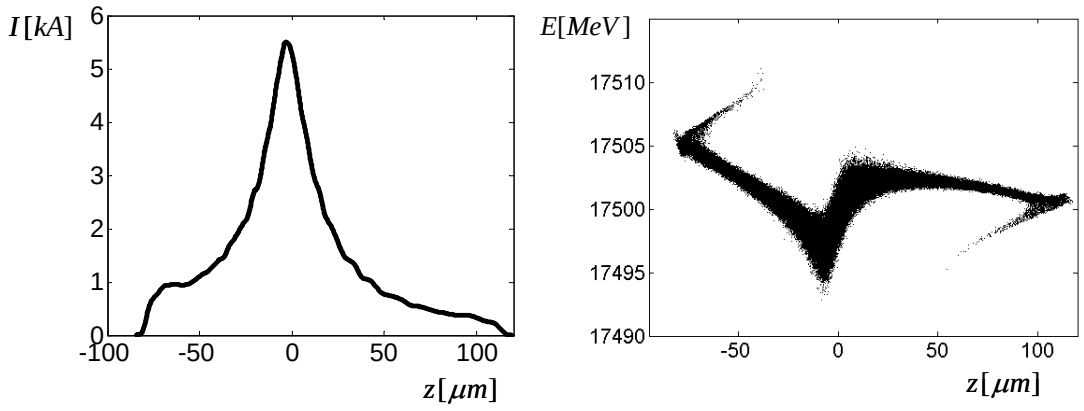

Fig. 1. Current profile and longitudinal phase space at the undulator entrance (1nC at 17.5GeV).

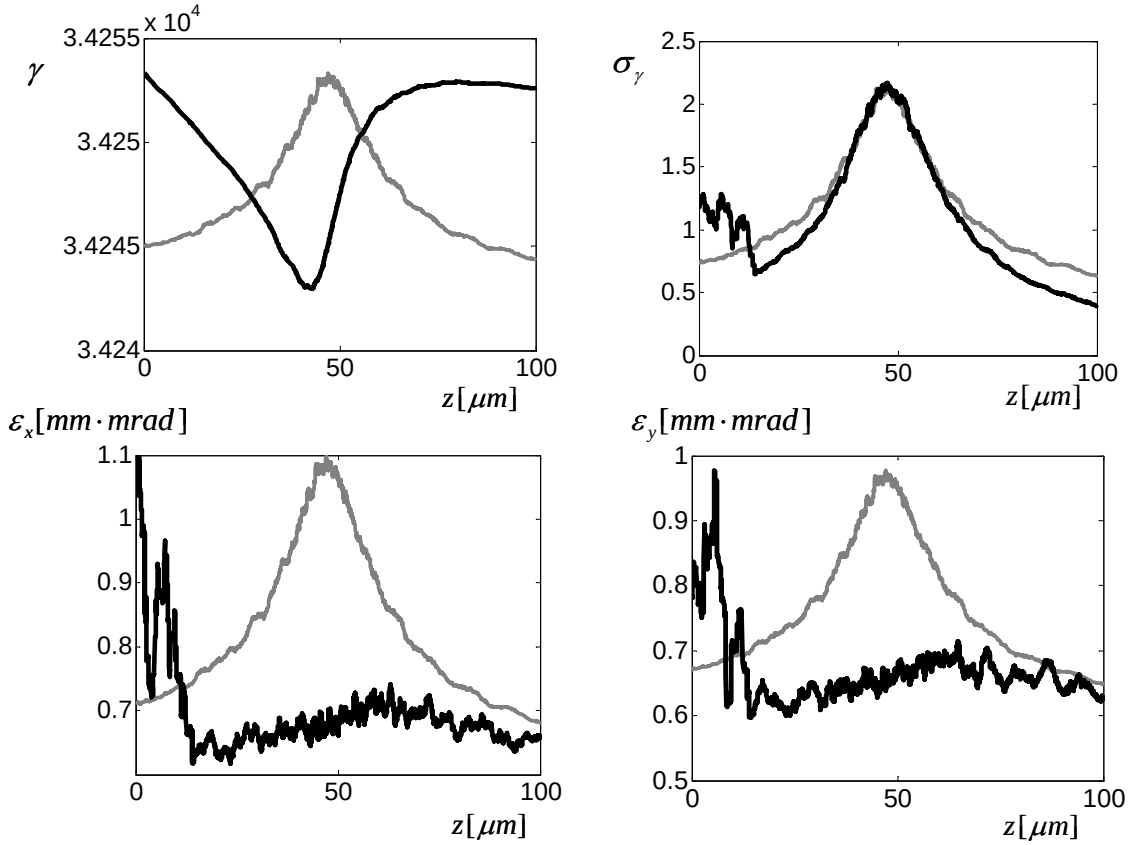

Fig. 2. Slice parameters of the bunch at the undulator entrance.

2. Wakefields in the Undulator

The effect of undulator wakefields becomes noticeable as gain reduction when the variation in energy becomes big compared to the FEL bandwidth, i.e. $\Delta E_{wake} / E \geq \rho$. In the case of SASE2 parameters [1] this gives the condition $W_z > 41 kV/(nC \cdot m)$ on the amplitude of wake potential per length.

There are three major sources of wakefields within the undulator: resistive walls, rough surfaces and geometric discontinuities. Resistive and surface roughness wakefields for beam pipes with smooth shallow corrugations have been calculated in [8]. It is found that the roughness of the investigated surface contributes similarly to the wake as an oxide layer ($\varepsilon_r \approx 2$) with 2% of the rms thickness of that roughness. An estimated rms thickness below 250 nm increases the surface effects by approximately 10% and is therefore neglected. The calculation of the geometrical and resistive wakefields is described in the following sections.

2.1. The Resistive-Wall-Wakefield

To estimate the resistive wall wakefields we use the results of [9]. For a round pipe of radius a the longitudinal impedance is given by

$$Z(k) = \frac{2}{ca}\left[\frac{\lambda}{k} - \frac{ika}{2}\right]^{-1}, \quad \lambda = \sqrt{\frac{2\pi|k|}{c}}\left[i + sign(k)\right], \tag{1}$$

where $k = \omega/c$ and ac conductivity $\tilde{\sigma}$ is given by

$$\tilde{\sigma} = \frac{\sigma}{1 - ikc\tau}.$$

We take radius $a = 3.8\,\text{mm}$ and consider this round pipe approximation as a pessimistic estimation of the wakefields for the elliptical pipe cross-section shown in Fig 4.

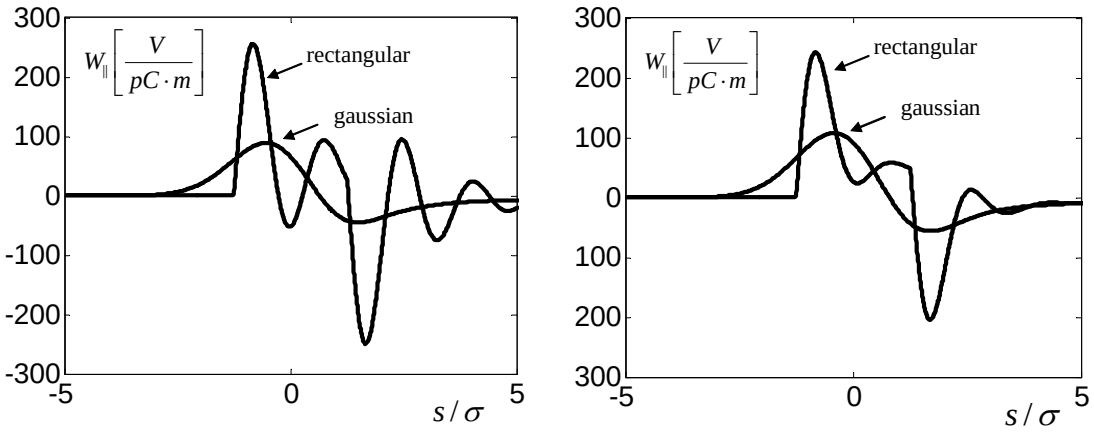

Fig. 3. Longitudinal wake potentials for copper (left) and aluminum (right).

The wakepotentials for two materials (copper: $\sigma = 5.8 \cdot 10^7 \left[\Omega^{-1} m^{-1}\right]$, $\tau = 2.46 \cdot 10^{-14} \left[\sec\right]$ and aluminum: $\sigma = 3.66 \cdot 10^7 \left[\Omega^{-1} m^{-1}\right]$, $\tau = 7.1 \cdot 10^{-15} \left[\sec\right]$) are shown in Fig. 3 and Table 1 for Gaussian bunch with RMS length $25 \mu m$ and for the rectangular shape of the same charge and peak current. A strong dependence of the wake amplitude on the bunch shape can be observed.

	Loss, V/pC/m	Spread, V/pC/m	Peak, V/pC/m
Gauss, cu/al	36/50	46/53	-89/108
Rect, cu/al	79/93	90/72	-256/243

Table 1. Parameters of the resistive wall wakepotentials.

2.2. The Effect of Geometrical Elements.

The beam tube inside of the undulator has elliptical cross section with a thin pumping slot along the whole undulator segment as shown in Fig. 4.

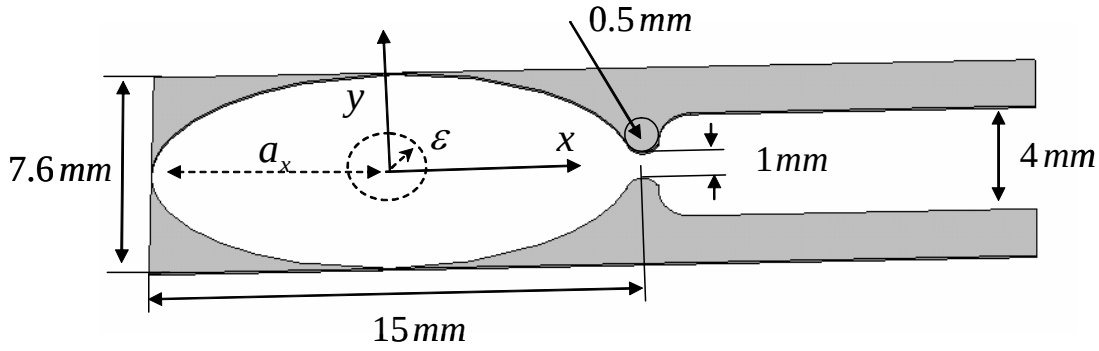

Fig. 4. The undulator pipe cross-section.

The theoretical results [10] based on Bethe's theory [11] are not applicable for this case while the width of the slot $w = 1mm$ is much bigger than the RMS length $\sigma = 25 \mu m$ of the Gaussian bunch used in the following calculations.

At the same time it is difficult to estimate the effect of the slot numerically as the effect is presumably small and numerical errors could spoil the numerical results. In order to obtain convincing estimation we have built a parametric model of the long slot and fitted the parameters of the model numerically [12]. The time-domain simulations with electrodynamics code ECHO [5] have been used for this purpose. Then we have extrapolated the numerical results from a treatable numerically set of parameters to the planned set and have compared the obtained results with energy method [13,14] based on electrostatic field calculations.

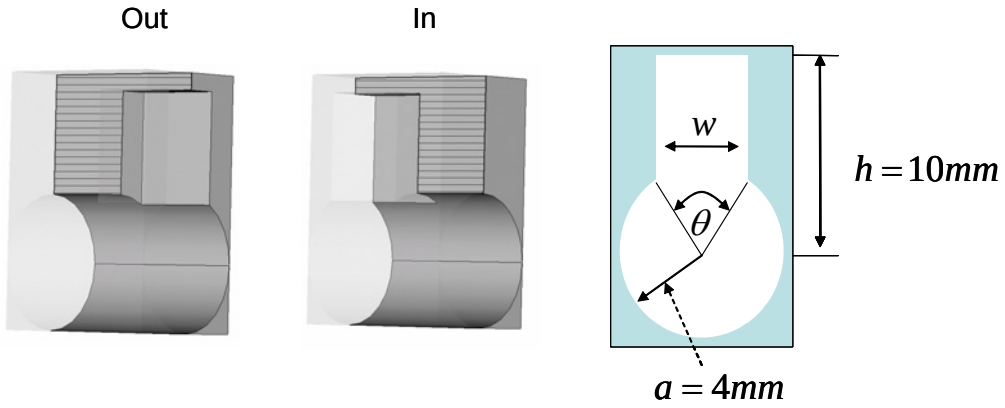

Fig. 5. The round pipe with very long longitudinal slot.

w [mm]	h [mm]	a [mm]	$\theta/2\pi$ [rad]	σ [μm]	„in“- transition loss [V/pC]	„out“ - transition loss [V/pC]
7	10	4	0.339	250	-0.16	3
1	20	7.5	0.021	25	-0.005	0.2

Table 2. The loss parameters for "out"- and "in"-transitions.

The numerical calculations shown in [12] results in the parametric model

$$k_{loss}^{out} = O(\theta^{1.8}\sigma^{-1}\ln(h/a)), \qquad k_{loss}^{in} = O(\theta/a). \tag{2}$$

From this model and the result of the first row in Tables 2 we obtain the second row of the table which gives the estimation

$$k_{loss} \simeq 0.2 \text{ V/pC}.$$

In order to check the prediction we recalculate the loss parameter by quite different energy method [13, 14]. As wake potential of the "in" transition is negligible we can write

$$W = 2W^e, \qquad W^e = \lambda_z(w_{ellipse} - w_{ellipse+slot}).$$

The accuracy of the energy method is checked by comparison with direct time-domain calculation for the structure shown in Fig 5. The results of the check are shown in Table 3.

w [mm]	σ [μm]	Loss factor from time-domain method [V/pC]	Loss from energy method [V/pC]	Difference [V/pC]
7	250	2.88	3.10	0.22
7	25	31.5	31.0	0.5
2	250	0.22	0.26	0.04
2	25	2.75	2.63	0.12

Table 3. Accuracy check for the energy method.

Next we apply the energy method to the structure shown in Fig. 1. Table 4 presents the calculated results obtained from 2D static solver (see [14] for details and notation).

ε [mm]	Mesh step [σ]	$\frac{2\pi w}{Z_0 c}$		
		Ellipse	Ellipse with slot	Difference
0.25	2	2.89161337	2.89165659	4.32e-5
0.25	1	2.90553777	2.90560728	6.95e-5

Table 4. Energy difference for two cross-sections.

From Tables 3, 4 we can conclude that

$$k_{loss} = 0.03 \pm 0.12 \text{ V/pC.}$$

The last result agrees well with the earlier obtained estimation. The kick factor on the axis can be estimated from the equation

$$W_y(s, x = y = 0) \approx \int_{-\infty}^{s} \frac{W(s', x = y = 0)}{a_x} ds'$$

as $k_{kick} < 0.001$ V/pC.

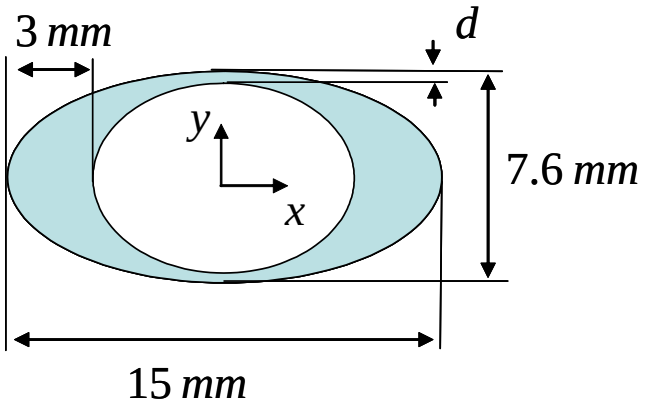

Fig. 6. The cross section of the absorber.

In order to protect the undulator from synchrotron radiation the absorbers should be installed in each undulator section. The absorber has the cross-section shown in Fig.6 and its length is 10 mm. We have considered two variants of absorber: $d = 0.5mm$ and $d = 0$. From direct time-domain calculations [5] the estimations for the loss and the kick factors are (in V / pC):

$$k_{loss} = 84, \qquad k_{kick,x} = 436 x/m, \qquad k_{kick,y} = 301 y/m$$

for $d = 0.5mm$ and

$$k_{loss} = 42, \qquad k_{kick,x} = 486 x/m, \qquad k_{kick,y} = -130 y/m$$

for $d = 0$.

To check the accuracy we have applied the energy method [13, 14] to the case $d = 0.5mm$ and have obtained $k_{loss} = 85\ V / pC$ on the axis that agrees with the previous result.

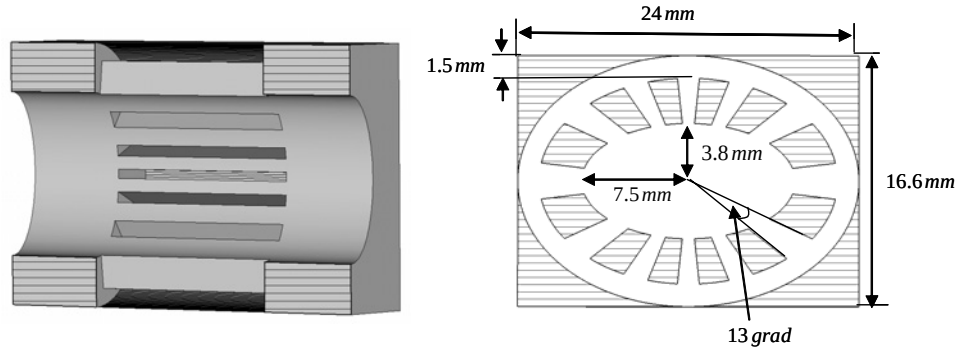

Fig. 7. The geometry of the pump.

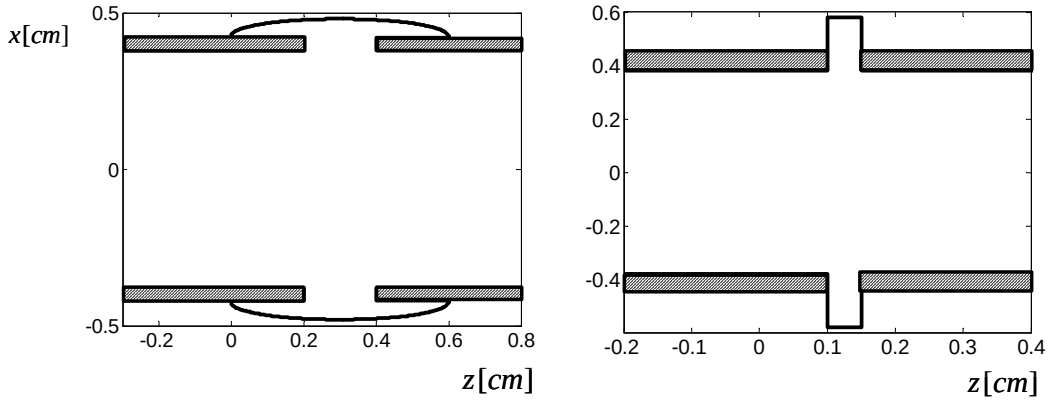

Fig. 8. The geometry of bellow (left) and flange gap (right).

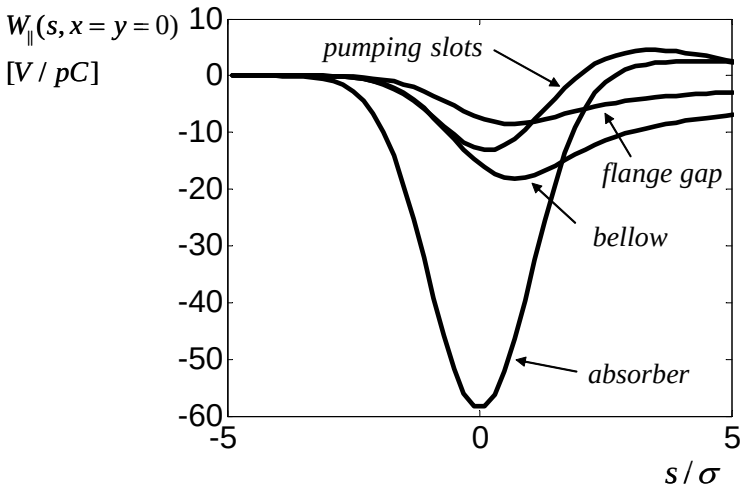

Fig. 9. Longitudinal wake potentials of the main elements.

The pump shown in Fig. 7 will be available in intersections. The longitudinal wakepotential of the pump calculated with 3D code [5] is shown in Fig. 9.

The wakes due to flange gap and below shown in Fig 9 are calculated in rotationally symmetric approximation for geometries outlined in Fig. 8.

	Loss, V/pC	Spread, V/pC	Peak, V/pC
absorber	42	16	-58
pumping slot (Fig.4)	<0.2	<0.1	>-0.3
pump (Fig.7)	9	4	-13
bellow	13	5	-18
flange gap	6	2.4	-8.5
Total geom.	**70**	**25**	**-95**

Table 5. Wake parameters.

The calculated wake parameters of the considered elements for Gaussian bunch with RMS length $\sigma = 25\mu m$ are gathered in Table 5.

2.3. Wakepotential for the Current Profile at the Undulator Entrance

The results calculated in the previous sections for copper pipe and Gaussian bunch with RMS length $\sigma = 25\mu m$ are shown in Fig. 10.

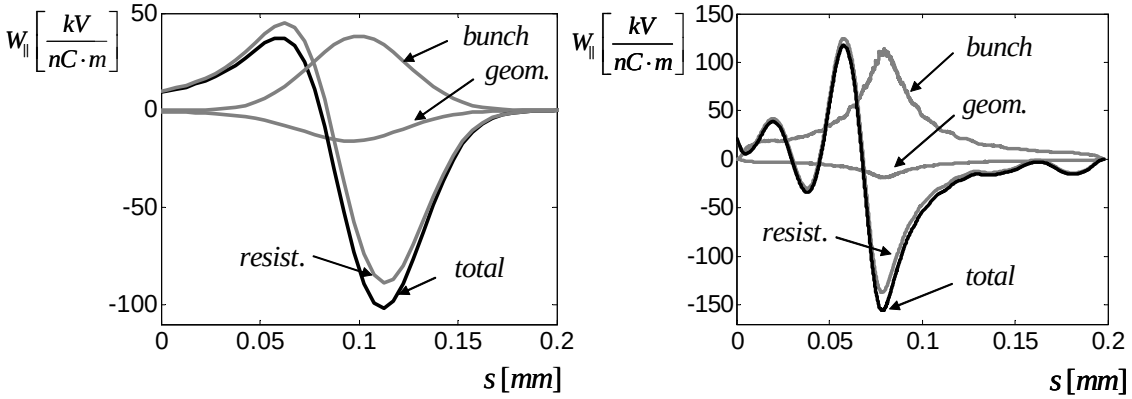

Fig. 10. Longitudinal wake potentials for Gaussian (left) and simulated (right) current profiles.

We see that the geometrical wake is resistive in the nature and since it can be written as

$$W_{\parallel}(s) = cZ_{hi}\lambda(s), \qquad (3)$$

where λ is the longitudinal bunch profile. From the fit of the above expression to the numerical results we have found that $Z_{hi} = 3.36[\Omega]$. Using Eq. 3 for the geometric wake and Eq. 1 for the resistive wall wake we have obtained the wake potentials for the simulated current profile (see Fig. 1). The wakes are shown in Fig. 10. The resistive wall wake is dominant and its amplitude depends strongly on the bunch shape.

3. Undulator-to-End Simulation

We have followed the standard way [15] of preparing input data for an FEL code: a macro-particle distribution at the undulator entrance was cut into longitudinal slices. A mean energy, RMS energy spread, current, RMS emittance were calculated for each slice. Then each slice was perfectly matched to the undulator entrance and all centroids were placed on the ideal orbit. The input parameters for GENESIS simulations are shown in Fig.2.

4. The FEL performance

In this section we evaluate with the help of code Genesis [4] the effect of wakefields on the XFEL performance for radiation wavelength 0.1 nm.

Parameter	symbol	unit	Value
radiation wavelength	λ	nm	0.1
Energy	E	GeV	17.5
energy spread	σ_E	MeV	1
undulator parameter	K_{rms}		1.97
Emmitance	ε_n	mm*mrad	0.7
peak current	I	kA	5
average beta function	β	m	17.25
undulator section length	L_{sect}	m	5
intersection length	L_{inters}	m	1.1
total length	L_{total}	m	260
undulator period	λ_u	m	0.048

Table 6. The SASE2 parameters.

A reliable method to increase the FEL undulator efficiency and compensate energy losses in the bunch consists in an adiabatic change of undulator parameters [16-18]. For a variable gap device, such as the TESLA FEL undulators, the on-axis magnetic field B_u is given by [1]

$$B_u = 3.694 \exp\left(-5.068 \frac{g}{\lambda_u} + 1.52 \left(\frac{g}{\lambda_u} \right)^2 \right),$$

where g means the undulator gap.

Hence, we can write

$$\frac{\Delta K_{rms}}{K_{rms}} \approx -\frac{\Delta g}{g} \left(-5.068 \frac{g}{\lambda_u} + 3.04 \left(\frac{g}{\lambda_u} \right)^2 \right),$$

where $K_{rms} = 93.4 \lambda_u B_u / \sqrt{2}$. For the given in Table 6 set of parameters we obtain a law for the gap change

$$\Delta g = -0.0124 \, \Delta K_{rms} / K_{rms}$$

and the efficiency parameter ρ [16] is equal to $7.1 \cdot 10^{-4}$.

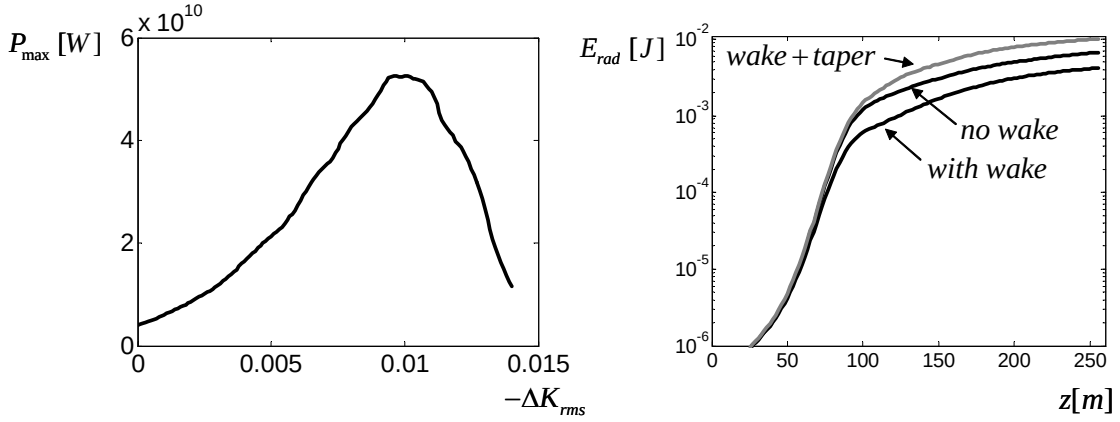

Fig. 11. The maximum power dependence on tapering (left) and the radiation power along the undulator (right).

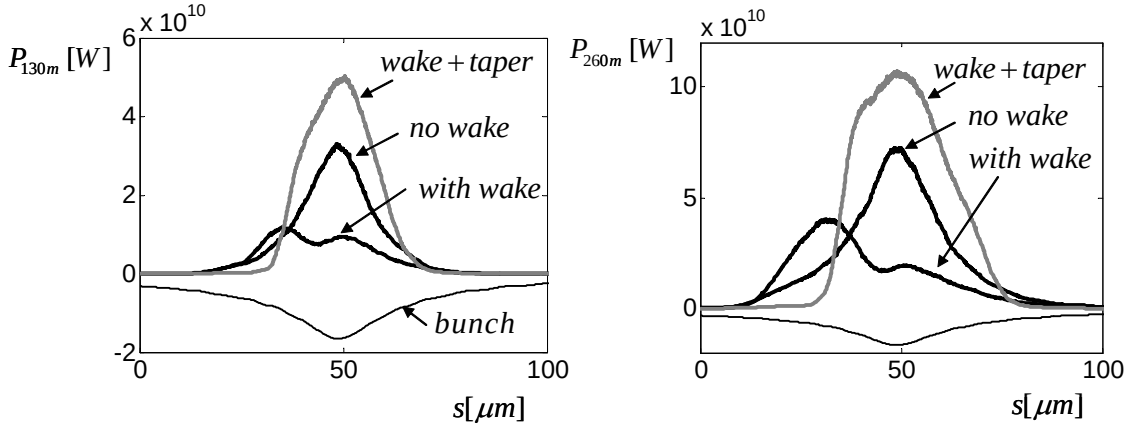

Fig. 12. The radiation power in the middle (left) and at the end of the undulator (right).

In order to find optimal taper for the calculated earlier wake potential we used the amplifier steady-state model with effective power of the shot noise [16]

$$W_{sh} = 3\rho \frac{W_b}{N_c \sqrt{\pi \ln N_c}} = 11800[W]$$

and energy loss $W_{\parallel} = 150 kV/nC/m$. The dependence of maximal power on change of the undulator parameter is shown in Fig. 11. The optimal taper is about

$$\Delta g = -0.0124 \Delta K_{rms} / K_{rms} = 60 \cdot 10^{-6} \, [m]$$

Next we have done numerical simulations of SASE FEL with bunch parameters shown in Fig 1, 2 and wake potential shown in Fig. 10. The calculated results are presented in Fig. 11-13.

As one can see from these figures, in the absence of wakefields the radiation pulse energy is 2.3 mJ at 130m. It is reduced to 1.2 mJ by undulator wakefields. The optimal linear undulator tapering $\Delta K/K \approx 7\rho$ allows to avoid the degradation and to increase the radiation energy up to 3.5 mJ at 130m.

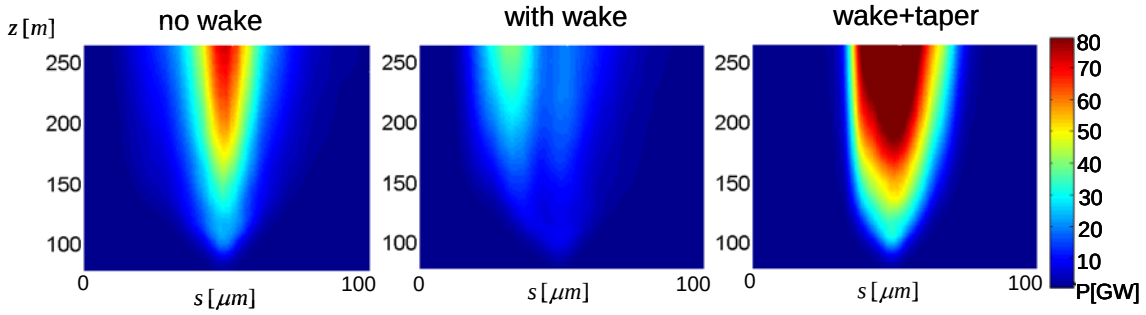

Fig. 13. Evolution of the power pulse along the undulator for the three considered cases.

Realization of the linear taper demands the undulator gap variation of only 60 μm per 260 m that imposes very severe tolerance requirements on the undulator alignment.

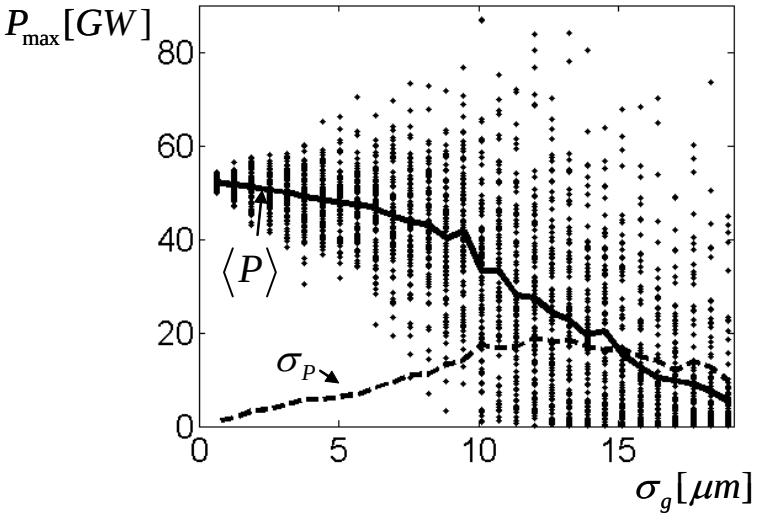

Fig. 14. Impact of statistical errors of undulator gap on power gain.

The undulator consists of 42 sections. In order to estimate tolerance requirements on undulator gap we have done series of steady state simulations where the optimal taper was disturbed by undulator gap error δg in each section. The gap error δg was distributed in accordance with Gaussian law

$$f(\delta g) = \frac{1}{\sqrt{2\pi}\sigma_g} \exp\left(-\frac{\delta g^2}{2\sigma_g{}^2} \right).$$

The maximal power of each seed together with mean power $\langle P \rangle$ and rms power deviation σ_P are shown in Fig. 14. The maximum of radiation power was found along first 130 meter of undulator. In the following we relate power degradation to the power P_0 obtained without gap errors. The RMS gap error of $\sigma_g = 10\ \mu m$ results in 20 % reduction of the expected radiation power:

$$\frac{P_0 - \langle P \rangle}{P_0} 100\% \approx 20\% \text{ at } \sigma_g = 10 \mu m$$

Taking into account the RMS power deviation σ_p (shown by dashed curve in the plot) we obtain that the pessimistic estimation $\langle P \rangle - 3\sigma_p$ constitutes about 80 % of the radiation power P_0 at $\sigma_g = 2\mu m$.

Conclusion

In this report we present calculations of the bunch shape at the undulator entrance in the European XFEL and the resulting wake fields in the undulator vacuum chamber. The shape of the bunch is smooth and quite close to the design parameters [1]. The wakes induced by the bunch in the undulator vacuum chamber are dominated by the resistive wall wake and reduce the radiation pulse energy by 50% in the case of an untapered undulator. Tapering the gap height linearly with a difference of 60 mm in the case of the 260 m long SASE undulator recovers and even slightly increases the radiated power compared to the un-tapered case without wake fields.

Acknowledgements

We would like to thank V. Balandin, R. Brinkmann, S. Reiche, E. Saldin, E. Schneidmiller and M. Yurkov for useful discussions.

References

[1] TESLA Technical Design Report, DESY 2001-011 (Hamburg, Germany, 2001)
[2] Flöttmann K., ASTRA User manual, http://www.desy.de/~mpyflo /Astra_dokumentation/
[3] Dohlus M., Methods for the Calculation of CSR Fields, TESLA-FEL-2003-05, DESY (2003)
[4] Reiche S., Nucl. Instrum. Methods Phys. Res., Sect.A, **429**, 3011 (1999)
[5] Zagorodnov I.A, Weiland T., Physical Review – STAB, **8**, 042001 (2005)

[6] Weiland T., Zagorodnov I., TESLA 2003-19, DESY (2003)
[7] Zagorodnov I., Weiland T., Dohlus M., TESLA 2004-01, DESY (2004)
[8] Dohlus M.,TESLA 2001-26, 2001.
[9] Bane K.L.F. and Stupakov G.V., SLAC-PUB-10707, 2004
[10] Stupakov G.V. Physical Review E, **51**, 4 (1995)
[11] Bethe H.A., Physical Review , **66**, 163 (1944)
[12] Zagorodnov I.A, http://www.desy.de/xfel-beam/data/talks/talks/zagorodnov_-_short_range_wakes_20050905.pdf
[13] Zotter B.W., Kheifets S.A., Impedances and Wakes in High-Energy Particle Accelerators (World Scientific, London, 1998)
[14] Bane K.L.F, Zagorodnov I.A, SLAC-PUB-11388, 2005
[15] Dohlus M. et al, Nucl. Instrum. Methods Phys. Res., Sect.A, **530**, 217 (2004)
[16] Saldin E.L.,Schneidmiller E.A., Yurkov M.V., The Physics of Free Electron Lasers (Springer, Berlin, 1999)
[17] Reiche S., Schlarb H., Nucl. Instrum. Methods Phys. Res., Sect.A, **445**, 155 (2000)
[18] Huang. Z., Stupakov G., Physical Review – STAB, **8**, 040702 (2005)